JOURNAL OF MATERIALS SCIENCE **38** (2003) 2679–2688

Structure and magnetic properties of nano-structured heterogeneous Au—Co alloys

V. Y. ZENOU
Nuclear Research Center Negev, PO Box 9001, Beer-Sheva 84190, Israel; Materials Sciences Division, Lawrence Berkeley National Laboratory, Berkeley, CA 94720, USA
E-mail: vyzenou@bezeqint.net

G. KUSINSKI
Materials Sciences Division, Lawrence Berkeley National Laboratory, Berkeley, CA 94720, USA; Department of Materials Science and Engineering, University of California, Berkeley, CA 94720, USA

L.YUE
Center for Materials Research and Analysis, University of Nebraska, Lincoln, NE 68515, USA

G. THOMAS
Materials Sciences Division, Lawrence Berkeley National Laboratory, Berkeley, CA 94720, USA; Department of Materials Science and Engineering, University of California, Berkeley, CA 94720, USA

High-resolution and analytical transmission electron microscopy, X-ray diffraction, magnetic and magnetoresistance measurements were used to investigate nanostructures of melt-spun $Au_{86}Co_{14}$ and $Au_{78}Co_{22}$ alloys. The microstructure of the $Au_{86}Co_{14}$ alloy was composed of very small Co precipitates inside the Au grains with some larger Co precipitates (20–35 nm) dispersed at the grain boundaries, while the microstructure of the $Au_{78}Co_{22}$ alloy consisted of Au/Co lamellar eutectic grains with Co precipitates (50–70 nm) dispersed at the grain boundaries. A few grains had very small (4 nm) Co precipitates. Annealing at 773 K for 10 min caused Co depletion in the Au matrix from 5.4–10 at.% to 0.9–2.0 at.%. Annealing also caused transitions from superparamagnetic to ferromagnetic and from single to multiple domain magnetic structure of some of the small and some of the larger Co precipitates, respectively. The MR ratios ($\Delta\rho/\rho$, in magnetic field of 14.5 kOe) of the as-cast $Au_{86}Co_{14}$ and $Au_{78}Co_{22}$ alloys were 2.5% and 2.6%, respectively. Annealing of the alloys at 673 K for 1 hr reduced $\Delta\rho/\rho$ to 0.9–1%.

1. Introduction

In 1988 it was discovered that the application of magnetic fields to artificially grown multilayered structures, consisting of alternating ferromagnetic and non-magnetic conductive layers, greatly reduced their electrical resistance [1]. This phenomenon is called giant magnetoresistance (GMR) [2].

In 1992, Xiao *et al.* [3] showed that GMR could also be observed in magnetic inhomogeneous media, in which magnetic granules are dispersed in a nonmagnetic metal matrix, such as Co precipitates in Cu or Ag. This new discovery gave the opportunity for further material development suitable for GMR applications. A comprehensive theory of GMR in granular materials has not yet been developed, although considerable information on the phenomenon has been obtained. For maximum GMR [4], the thickness of the ferromagnetic and non-magnetic layers (or the size of the ferromagnetic precipitates [5] and non-magnetic spacing between the precipitates in the inhomogeneous media) are no more than a few nm, that is less than the mean free path for inelastic scattering of the conduction electrons. There is considerable evidence [4, 6–8] that spin-dependent scattering, of conduction electrons at interfaces between the ferromagnetic layers and non-magnetic matrix, dominates in many cases.

Melt spinning is the commonly used method to obtain a fine dispersion of Co in Au. The eutectic decomposition[6] in the Au—Co system promotes the formation of a multilayered microstructure, showing GMR [9, 10]. A few investigators [11–13] used water quenching of a solid-solution of Au—Co alloys followed by annealing, instead of melt spinning, in order to obtain an even finer microstructure of coherent Co precipitates (up to 4 nm) dispersed in the Au matrix. This work will show that both microstructures (relatively large Co precipitates and lamellae and fine coherent Co precipitates) co-exist in our as-cast samples.

In order to improve the GMR, a detailed understanding of the influence of the microstructure on the magnetic properties is necessary. In this paper, the Au—Co system was chosen to study the correlation between

the microstructure, the magnetic and the GMR properties of melt-spun ribbons. Au–Co is not one of the important heterogeneous systems for GMR [6]; however, the large difference in atomic scattering factor (~2 ratio) and the large lattice misfit (~13%) between Au (fcc) and Co (fcc) make it an excellent choice for transmission electron microscopy (TEM) imaging and high resolution TEM (HRTEM) imaging.

2. Experimental procedure

The equilibrium phase diagram of Au–Co is shown in Fig. 1. As shown, the Au–Co system exhibits an eutectic liq. $\leftrightarrow$ Au + Co at 24.8 at.% Co and 1269.5 K. The maximum solubility [14] of Co in Au is 23 at.% at the eutectic temperature. The high-temperature fcc solid solution (α-Co) has a maximum solubility of 2.5 at.% Au at 1473 K. The low-temperature hcp solid solution (ε-Co), stable below 695 K, has a very limited solubility of Au (<0.05 at.%). Fig. 1 also shows the calculated points for chemical spinodals and coherent spinodals as was calculated by Hütten *et al.* [9].

$Au_{86}Co_{14}$ and $Au_{78}Co_{22}$ alloys were prepared by arc melting. The ingots were subsequently melt-spun in an argon atmosphere using a Cu wheel with a tangential velocity of 30 m/s. The obtained ribbons were 10–20 cm long, 2 mm wide and 30–40 μm thick. Wet chemical analysis showed that the measured compositions were close to the nominal compositions (14.1 and 21.8 at.%, for 14 and 22 at.%, respectively). X-ray diffractions showed that both sides of the ribbon were crystalline with no evidence of amorphous areas.

The samples were vacuum annealed in a conventional tube furnace at different temperatures (573–873 K) for 10 min and also at 673 K temperature for 2, 5, 10, 30, 60 and 120 min. Magnetic measurements were performed at room temperature in a Lake Shore model 7300 vibration magnetometer system in fields up to 15 kOe. Thermomagnetic analyses were performed using a Perkin-Elmer TGA-7 instrument. A customary four-point probe was used to determine resistance at temperatures of 20–25 K and magnetic fields up to 14.5 kOe. The magnetic field during measurements was applied parallel to measuring current through the sample. Transmission electron microscopy, including high-resolution imaging, electron diffraction, electron microdiffraction, chemical microanalysis (EDX) and energy-filtered (EELS) imaging, were carried out at the National Center for Electron Microscopy (NCEM) at the Lawrence Berkeley National Laboratory.

The EDX analysis was performed in two microscopes: Jeol 200 CX and Philips CM 200. The probe size (beam diameter) was 9–17 nm and 1.2–1.4 nm in the Jeol 200 CX and Philips CM200, respectively. The k factors were determined experimentally at Jeol 200 CX (measurement's relative accuracy: 1%). Calculated k factors were used at the Philips CM 200 (semi-quantitative; measurement's relative accuracy: 10%). Since very small Co precipitates (1–2 nm and up) were dispersed in the Au matrix a caution had to be taken while measuring the Au matrix composition. Emispec analytical PC software (EM vision 3.2) was used for the analysis and also to track the drift. The magnetic domain structure was investigated using a Lorentz TEM imaging (L-TEM) in a Phillips CM 200 FEG microscope with a weakly excited objective lens and a Gatan imaging filter (GIF), with a 1 k × 1 k CCD camera. Additionally, in-situ heating experiments were performed in a JEOL 200 CX TEM using a Gatan 628-Ta heating stage, to observe microstructural changes.

In order to obtain electron transparent thin samples, pieces up to 3 mm were cut out from the ribbons. After dimpling from one side samples were mounted on 3 mm copper rings and dimpled from the other side. Ion-milling was performed in two stages (at liquid nitrogen temperature): first by thinning at 5 kV with gun current of 6.5 mA, from both sides, and at an incident angle of 10°, until the first hole appeared, followed by thinning at 2 kV at an incident angle of 6–8°. Crystallographic structural data was obtained by X-ray diffraction using Cu K_α radiation. A Rietveld PC program (Young's DBWS-9411 [15]) was used to analyze the obtained data.

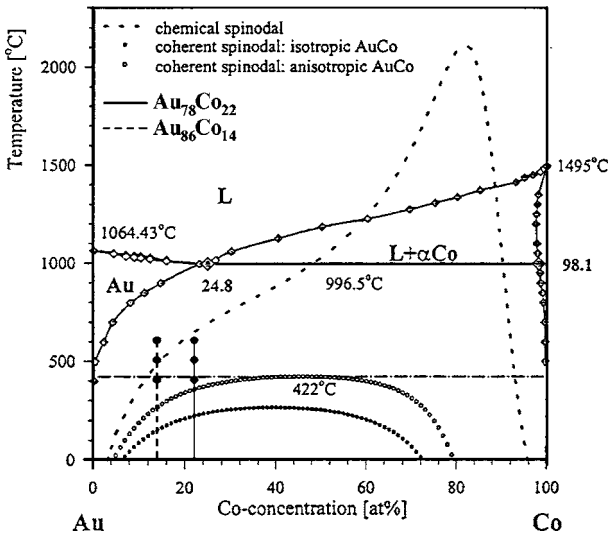

Figure 1 Equilibrium phase diagram of Au–Co compared with the calculated chemical and coherent spinodals (from [9]). The nominal compositions of the investigated melt-spun ribbons, as well as the annealing temperature, are shown.

3. Results and discussion

3.1. Microstructural investigation as-cast and during annealing

3.1.1. $Au_{78}Co_{22}$ as-cast

TEM images, as shown in Fig. 2a, showed that the microstructure of the as-cast $Au_{78}Co_{22}$ consisted of grains (1–2 μm size) with a lamellar (multilayered) eutectic structure of Au and Co. Co precipitates (50–70 nm) were observed at the grain boundaries (Fig. 2a and b). Fig. 2c shows the Au/Co lamellar eutectic structure, with 10–20 nm width Co lamellae. Selected area electron diffraction confirmed the crystallographic structure of both the Co and the Au lamellae as fcc. The high-temperature [14] stable fcc Co can dissolve up to 2.5 at.% Au while the low-temperature stable hcp Co can not dissolve more than 0.05 at.%. This small

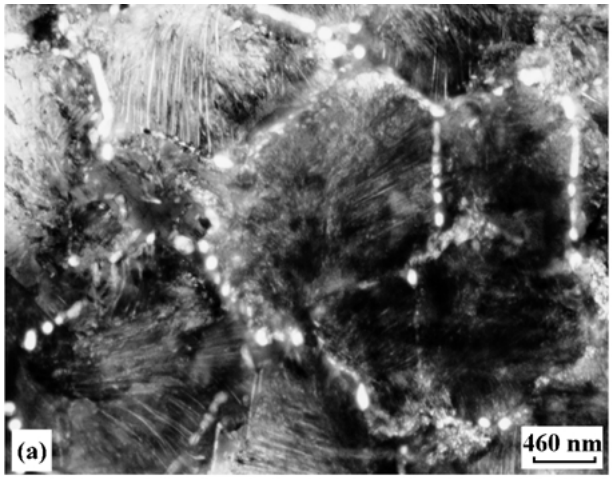

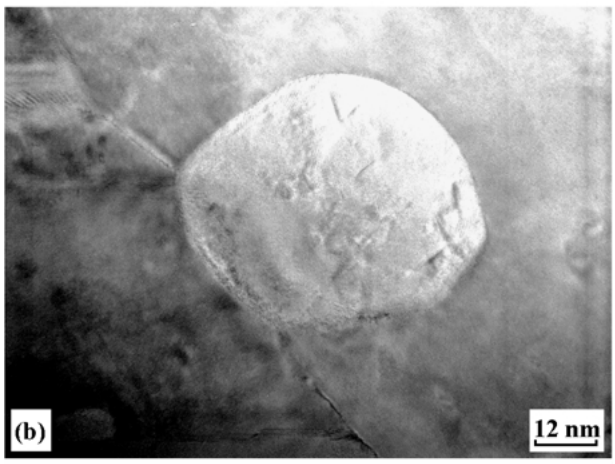

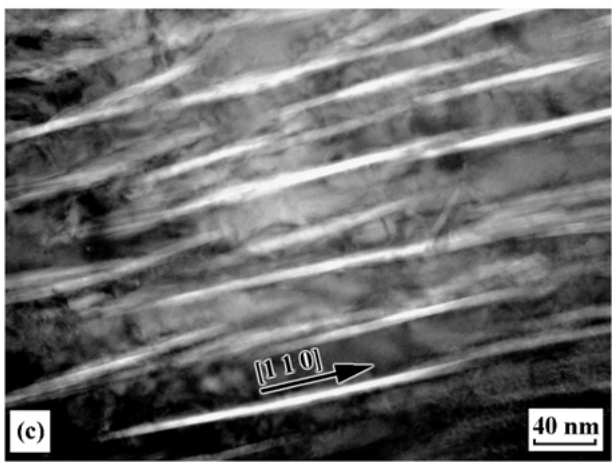

Figure 2 Bright field electron images of the microstructure of $Au_{78}Co_{22}$ alloy: (a) Au/Co lamellar eutectic grains with Co precipitates dispersed at the grain boundaries, (b) Co precipitate within grain boundary, and (c) Au/Co lamellar eutectic structure.

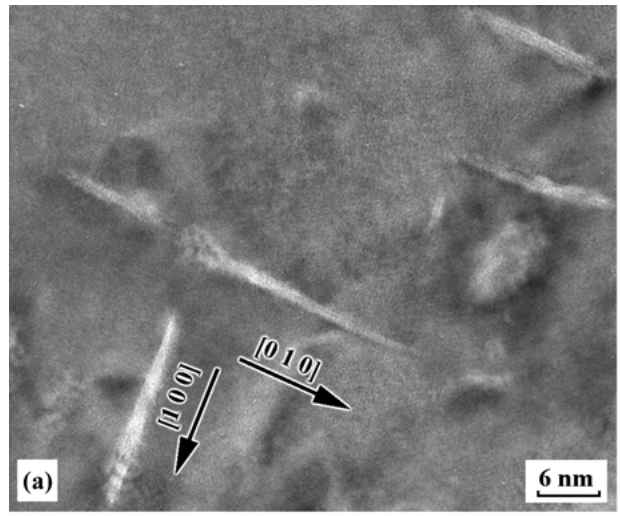

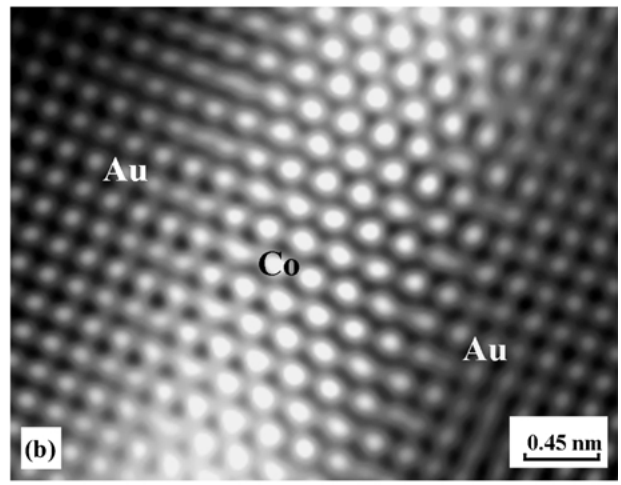

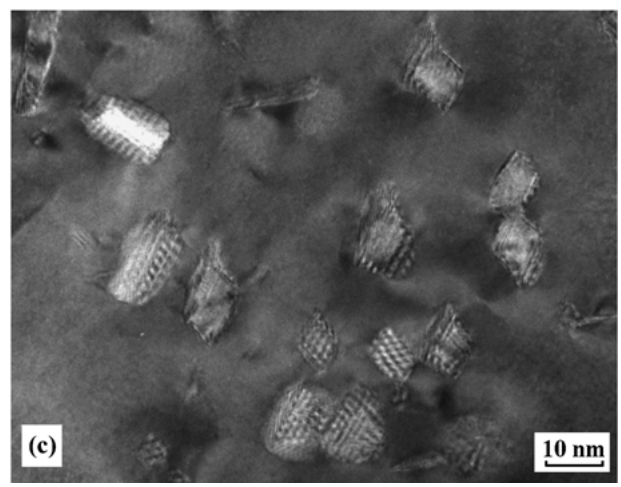

Figure 3 High-resolution images demonstrating fine Co precipitates in the $Au_{78}Co_{22}$ alloy: (a) 1–2 nm wide elongated Co precipitates, (b) lattice image of part of differently oriented Co precipitate with the Au matrix $((0\,0\,1)_{Au}||(1\,1\,1)_{Co}$; $[1\,0\,0]_{Au}||[0\,1\,-1]_{Co}$, with 2° rotation around $[0\,0\,1]_{Au}$), and (c) small faceted Co precipitates that were found at other grains showing moiré fringes.

amount of Au in Co, during solidification at high cooling rates, may metastabilize the fcc Co phase at room temperature.

The Co lamellae were aligned in $\langle 1\,1\,0\rangle_{Au}$ directions, and had the orientation relationship $((0\,0\,1)_{Au}||(0\,0\,1)_{Co}$ and $[1\,0\,0]_{Au}||[1\,0\,0]_{Co}$, with 2° around $[0\,0\,1]_{Au}$). Similar structures were observed in melt spun $Au_{83.3}Co_{16.7}$ as reported by Bernardi *et al*. [16]. In addition, fine (1–2 nm in width) coherent elongated secondary Co precipitates were found (Fig. 3a) by HRTEM. Such Co precipitates were aligned in $\langle 1\,0\,0\rangle_{Au}$ directions and had the same orientation relationship as the Co lamellae. Similar precipitates were observed in $Au_{90}Co_{10}$ [11] and $Au_{80}Co_{20}$ [13] bulk alloys prepared by water-quenching followed by annealing at 573 K for 1 hr. A few precipitates had a different orientation relationship $((0\,0\,1)_{Au}||(1\,1\,1)_{Co}$; $[1\,0\,0]_{Au}||[0\,1\,-1]_{Co}$, with 2° around $[0\,0\,1]_{Au}$, Fig. 3b). The reason for the different orientation relationship is not clear at this stage of the research.

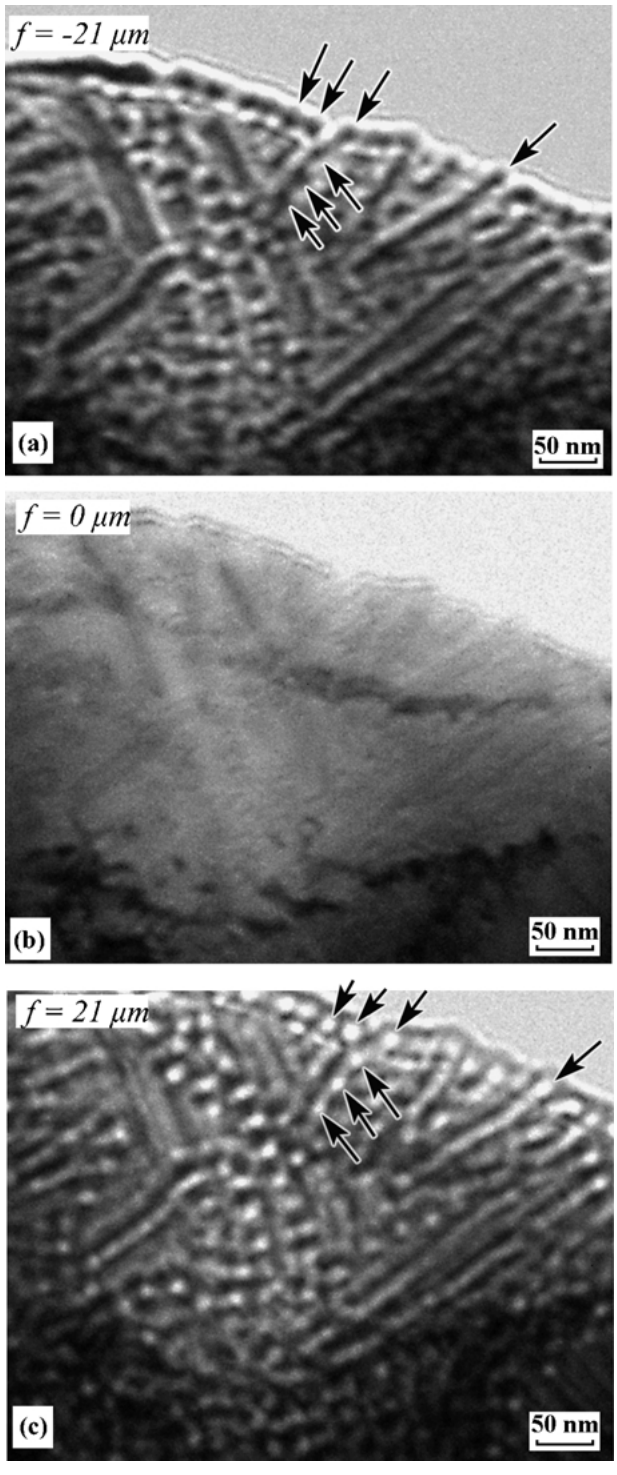

Figure 4 Lorentz imaging (Fresnel method) of Co precipitates in $Au_{78}Co_{22}$ alloy. (a–c) Different focus images. Few arbitrary precipitates are marked with arrows for contrast comparing. The black round areas surround with white rings in under-focus (a) that reverse to white round areas surround with black rings in over-focus (c) image indicate that the Co precipitates have a single domain magnetic structure. This contrast reverse is in agreement to simulation made for a single domain particles with a curling-like magnetization in [7].

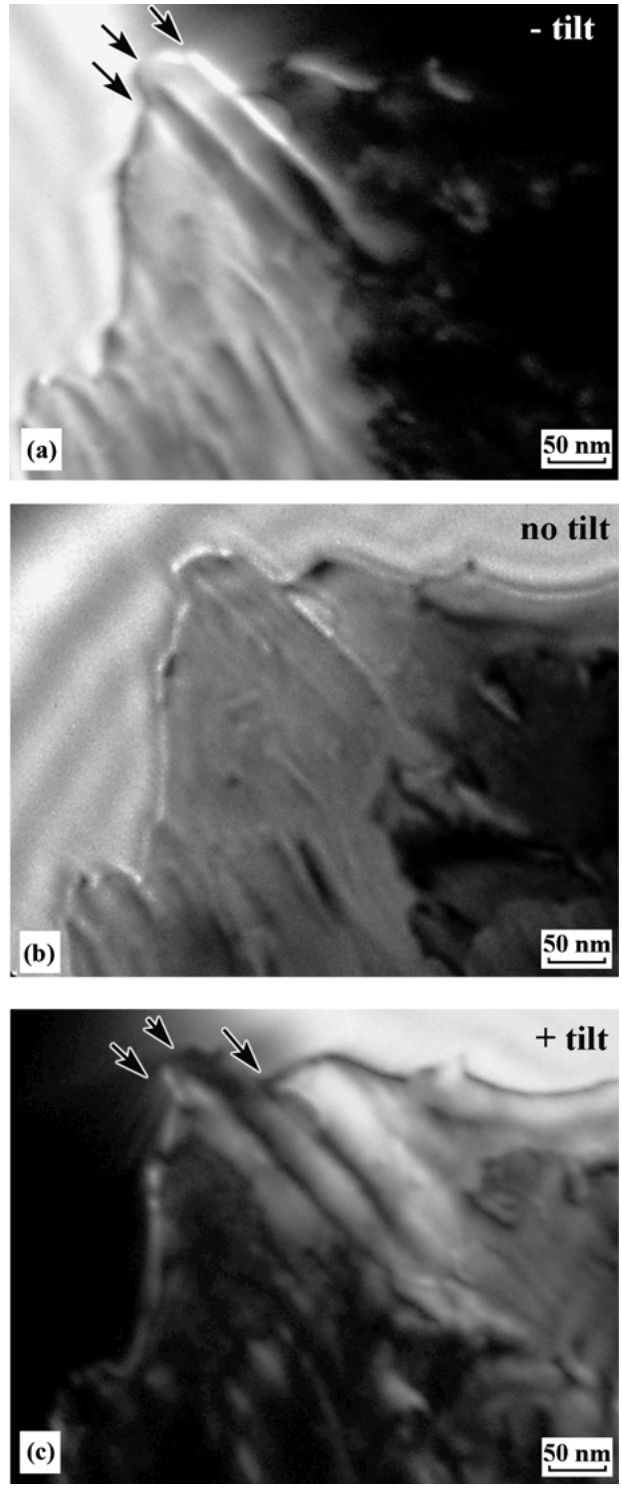

Figure 5 Lorentz imaging (Foucault method) of Co lamellae (marked with arrows) at $Au_{78}Co_{22}$ alloy. (a–c) Different tilt images. The contrast changes are consistent with single magnetic domain Co lamellae.

Moreover, some grains had small (4 nm and up; Fig. 3c) faceted Co precipitates instead of the eutectic structure. These small faceted Co precipitates, with a well-defined interface with the Au matrix, were reported earlier [12] for $Au_{80}Co_{20}$ bulk alloy prepared by water-quenching, followed by annealing at 773 K for 1 hr.

Finally, some of the Co precipitates found at the grain boundaries contained small Au spheres inside them, as identified by their $(1\,1\,1)_{Au}$ interplanar distances in HRTEM. The average diameter of these Au spheres was 3.5 nm.

From Lorentz TEM (L-TEM) imaging of the $Au_{78}Co_{22}$ alloy it was found that both Co precipitates (Fig. 4, Fresnel method) and the lamellae (Fig. 5, Foucault method) had a single magnetic domain structure. Similar Co precipitates, with the same magnetic (Fresnel method) contrast, were found in a single

TABLE I Co concentration in the Au matrix measured by EDX microanalysis. The Co concentration was also calculated using Vegard's law and Au lattice parameter measurements

	at.% Co			
	$Au_{78}Co_{22}$ alloy		$Au_{86}Co_{14}$ alloy	
Annealing parameters	EDX	X-ray diffraction	EDX	X-ray diffraction
As-cast	[a]5.4 ± 0.5	6.6	[b]10.0 ± 1.0	9.4
673 K/120 min	–	–	[a,b]3.3 ± 0.1	–
773 K/10 min	[a]0.9 ± 0.3	1.5	[a]2.0 ± 0.6	1.5

[a]Philips CM 200; 1.2–1.4 nm probe size, calculated k factors.
[b]Jeol 200 CX; 9–17 nm probe size, experimentally k determined factors.

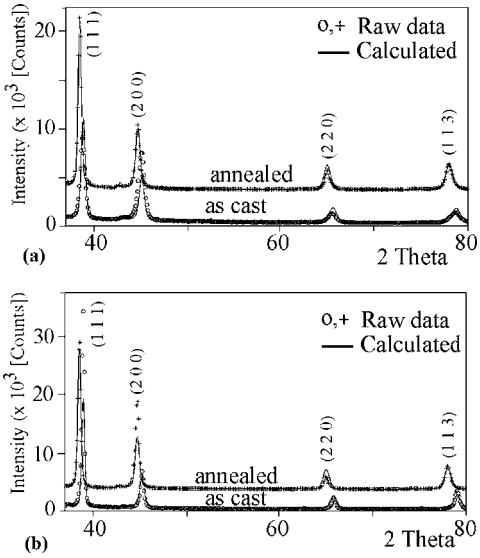

Figure 6 (a, b) Rietveld analysis of the X-ray diffraction data of $Au_{78}Co_{22}$ alloy (a) and $Au_{86}Co_{14}$ alloy (b) before and after 773 K/10 min annealing. The measured data is represented with 'o' or '+' symbols while the calculated profile are represented with a solid line.

domain state with a curling-like magnetization [7]. To our knowledge this is the first direct observation of single magnetic domain lamellar (eutectic) structures.

The Co concentration in the Au matrix measured by EDX microanalysis was found to be 5.4 ± 0.5 at.% (Table I). Rietveld analysis (Fig. 6a) of the X-ray diffraction data showed the Au lattice parameter to be 0.40427 nm. This value is lower than that reported in the literature for pure Au (0.4078 nm). The measured Au unit cell shrinkage is due to the dissolved Co in the Au and has been reported elsewhere [10]. From Vegard's law it is estimated that the Au matrix dissolves about 6.6 at.% Co. Okamoto *et al.* [14] reported a positive deviation from Vegard's law: using other experimental techniques, they found that more Co were dissolved in the Au matrix than would be expected from Vegard's law.

3.1.2. $Au_{78}Co_{22}$ during in situ TEM annealing

The changes in the microstructure of the $Au_{78}Co_{22}$ alloy during annealing from room temperature to 873 K were investigated by *in situ* TEM. The results are shown in Fig. 7. During annealing (at 873 K) most of the Co

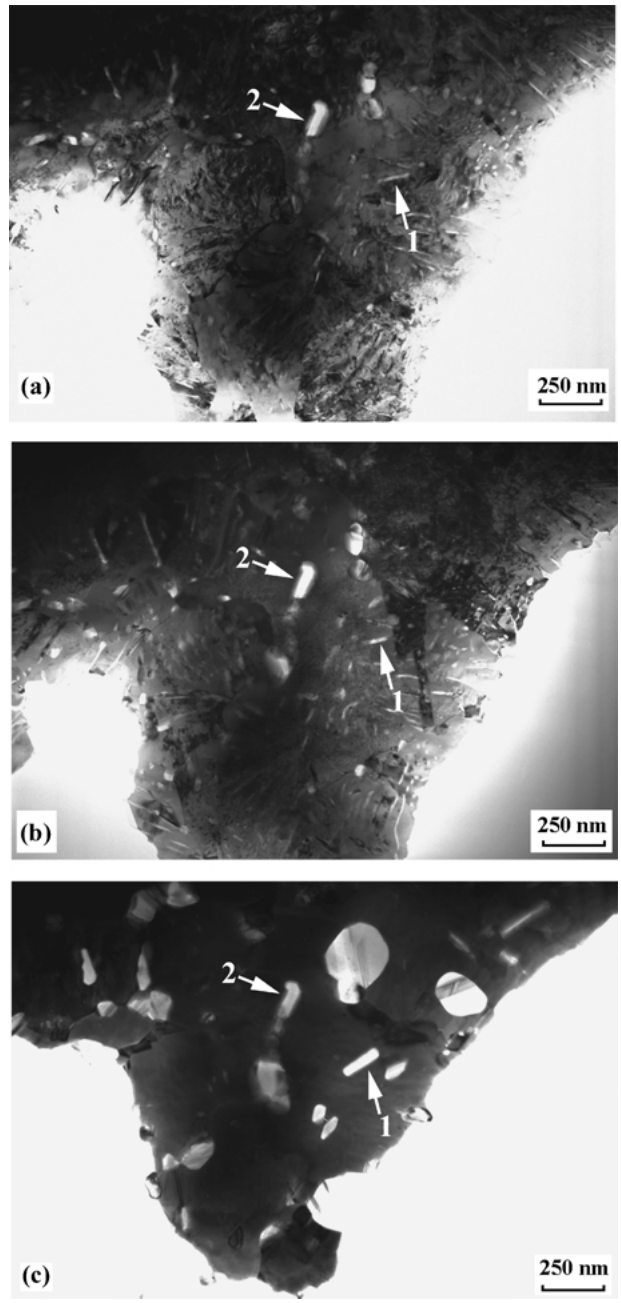

Figure 7 Bright field electron images demonstrating the microstructure of $Au_{78}Co_{22}$ alloy during annealing: (a) As-cast, (b) after 3 min annealing at 673 K, and (c) after 10 min annealing at 873 K.

lamellae disappeared while the Co precipitates and the remaining Co lamellae grew. For instance the width of the Co lamella, marked as "1" in Fig. 7, grew from 10.0 nm (as-cast) to 12.7 and 28.8 nm after annealing at 673 K for 3 min and at 873 K for 10 min, respectively, while the length grew from 89 nm (as-cast) to 110 nm after 10 min annealing at 873 K. However, the Co precipitate, marked "2" in Fig. 7, did not grow. From the single variant stacking fault contrast the larger Co precipitate shown in Fig. 7c (upper right) is concluded to be hcp. L-TEM showed that the large precipitates (200 nm) had a multi-domain magnetic structure, as was reported in an earlier investigation [6].

EDX microanalysis revealed that annealing at a temperature of 773 K reduced the Co concentration in the Au matrix to 0.9 ± 0.3 at.%. However, Rietveld analysis of the $Au_{78}Co_{22}$ diffraction data gave the Au lattice

parameter as 0.4070 nm, from which we arrived to an estimation of 1.5 at.% Co dissolved in the Au matrix.

3.1.3. $Au_{86}Co_{14}$ as-cast

The microstructure of the $Au_{86}Co_{14}$ alloy, shown in Fig. 8a, differed from the microstructure of the $Au_{78}Co_{22}$ alloy. Only a few grains had the Au/Co lamellar structure. The widths of the Co lamellae were between 3.5 and 14 nm. The amount and size of the Co precipitates found at the grain boundaries were smaller (20–35 nm, Fig. 8b) than those found in the $Au_{78}Co_{22}$ alloy. Moiré fringes around the Co precipitates indicated that they were lens-shaped, while microdiffraction showed that the Co precipitates were fcc single crystals. As can be seen from Fig. 8a, small black dots were found inside the grains. They could not be identified by HRTEM and could only be seen at specific orientations, which indicate very small Co precipitates seen only by strain contrast [17]. Some of these dots had a faceted shape, exactly like those found in $Au_{78}Co_{22}$ (Fig. 3c). As will be reported below, annealing caused these precipitates to grow (Fig. 8c).

L-TEM showed that in the as-cast samples all of the Co precipitates had a single magnetic domain structure.

The Co concentration in the Au matrix was measured by EDX microanalysis and was found to be 10.0 ± 1.0 at.%. In agreement, the Au lattice parameter determined from the X-ray diffraction data using Rietveld analysis was 0.40278 nm, which lead to an estimation of 9.4 at.% Co dissolved in the Au matrix.

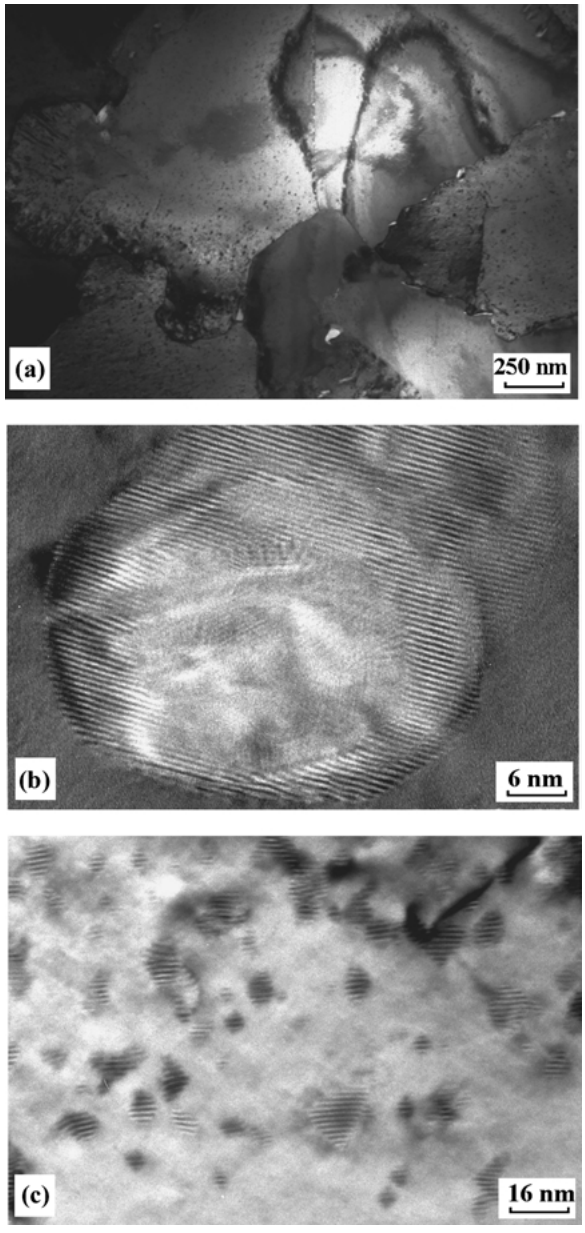

Figure 8 Bright field electron images of $Au_{86}Co_{14}$ alloy. (a) Grains with Co precipitates dispersed at the grain boundaries and small 'black dots', (b) one of the Co precipitates that was found at grain boundary with moiré fringes around it, and (c) after 10 min annealing at 773—the 'black dots' grew and showed moiré fringes.

3.1.4. $Au_{86}Co_{14}$ during in situ TEM annealing

The changes in the microstructure of the $Au_{86}Co_{14}$ alloy during annealing at 673 K were investigated by *in situ* experiments in the TEM. It was found that the precipitates more than doubled after 120 min annealing. Microdiffraction revealed that some of the small Co precipitates (15–25 nm, Fig. 9a) were hcp crystals while the larger Co precipitates (Fig. 9b) and lamellae (Fig. 9c) were fcc single crystals. To our knowledge, this is the first time that hcp ε-Co has been found in melt-spun or water-quenched hypoeutectic Au–Co alloys. Before annealing, all of the Co precipitates that were examined had the fcc structure. This phenomenon is currently under investigation but possible explanations are that there was an fcc to hcp transformation (with shorter Au diffusion paths in the smaller Co precipitates) or hcp ε-Co precipitation from the matrix during the annealing. Annealing at 773 K for 10 min caused the growth of some of the small 'black dots' Co precipitates (discussed above), which now could be resolved from their moiré fringes (Fig. 8c).

From EDX microanalysis it was found that the Au matrix contained 3.3 ± 0.1 at.% Co after annealing at 673 K for 120 min and 2.0 ± 0.6 at.% Co after annealing at 773 K for 10 min, respectively. Rietveld analysis of the X-ray data for the $Au_{86}Co_{14}$ annealed at 773 K for 10 min revealed a 0.4070 nm Au lattice parameter, giving 1.5 at.% Co dissolved in the Au matrix. Thus, during the annealing process, Co atoms segregate from the Au-matrix, leading to coarsening of some of the Co precipitates.

3.2. Magnetic properties

The dependence of saturation magnetization (M_s) and coercivity (H_c) as a function of annealing temperature at a 10 min annealing time and as a function of the annealing time at 673 K are presented in Figs 10 and 11, respectively.

The saturation magnetization of both samples increased with an increase in annealing temperature up to 723 K (Fig. 10a) and in annealing time up to 5 min at 673 K (Fig. 11a), in agreement with previously published results [6, 7]. The reason for this increase is the Co precipitation out from the Au matrix. The depletion

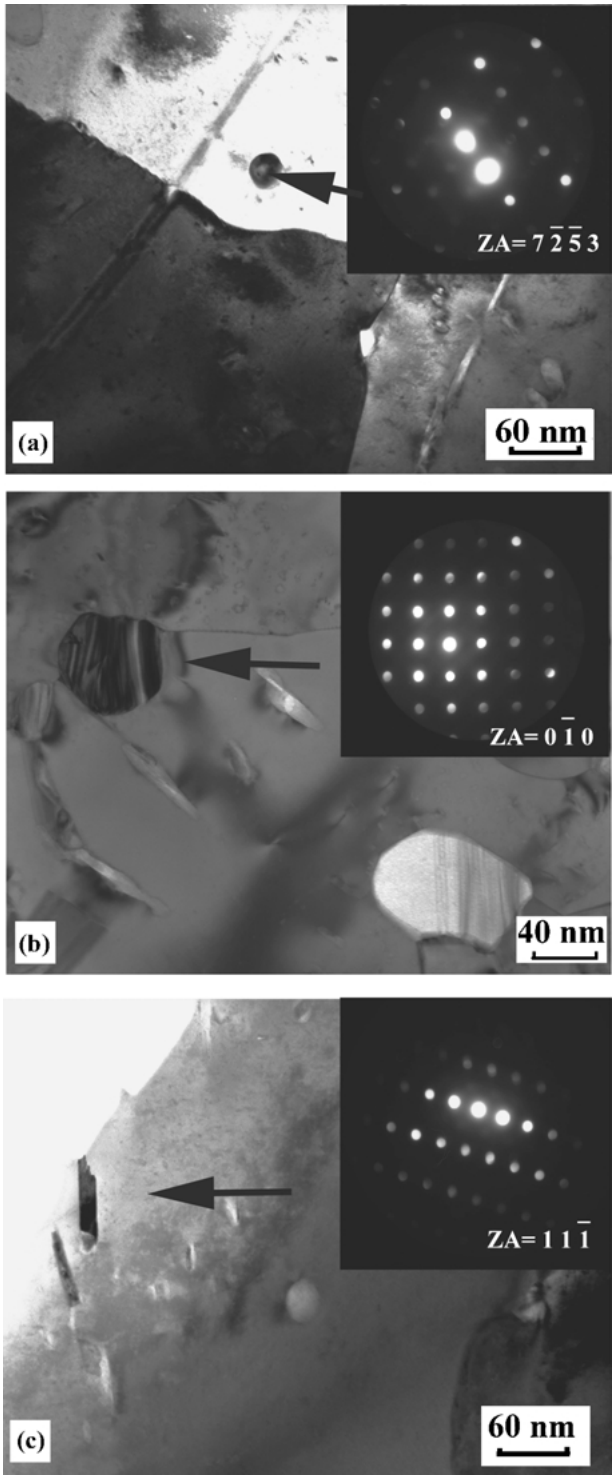

Figure 9 Co precipitates in $Au_{86}Co_{14}$ alloy: (a) Small hcp Co precipitate, (b) Fcc Co precipitate, and (c) Fcc Co lamella. Microdiffractions of the dark (due to diffraction contrast) Co precipitates are shown at the upper right of each image.

of Co in the Au matrix was reported above. The critical diameter, D_c, at which a spherical precipitate becomes ferromagnetic has been estimated to be 3.8 nm at room temperature [6]. Since some Co precipitates were smaller than that value and annealing caused to growth of Co precipitates it is reasonable that some of these small precipitates had a transition from superparamagnetic to ferromagnetic while growing. Since smaller magnetic fields are required to saturate ferromagnetic particles compared to superparamagnetic

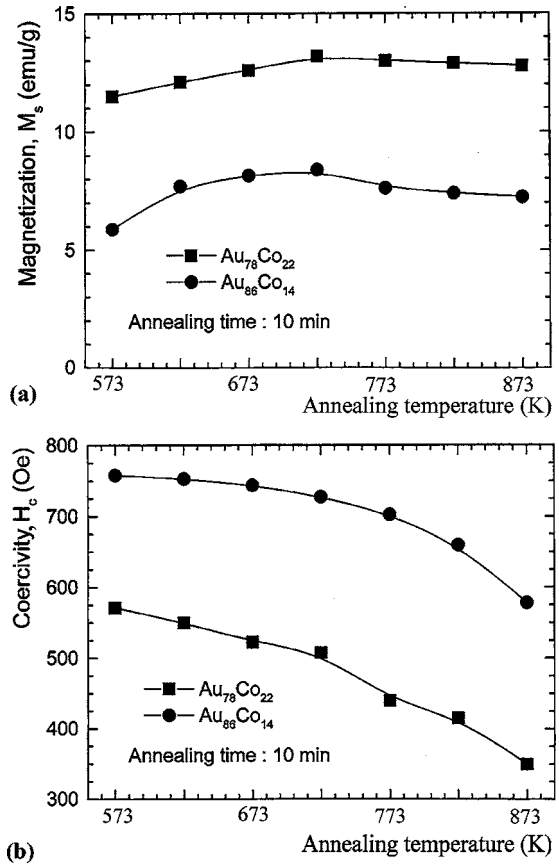

Figure 10 The magnetic properties of $Au_{78}Co_{22}$ and $Au_{86}Co_{14}$ (measured at room temperature) as a function of annealing temperature (for 10 min). (a) Saturation magnetization (M_s) and (b) Coercivity (H_c).

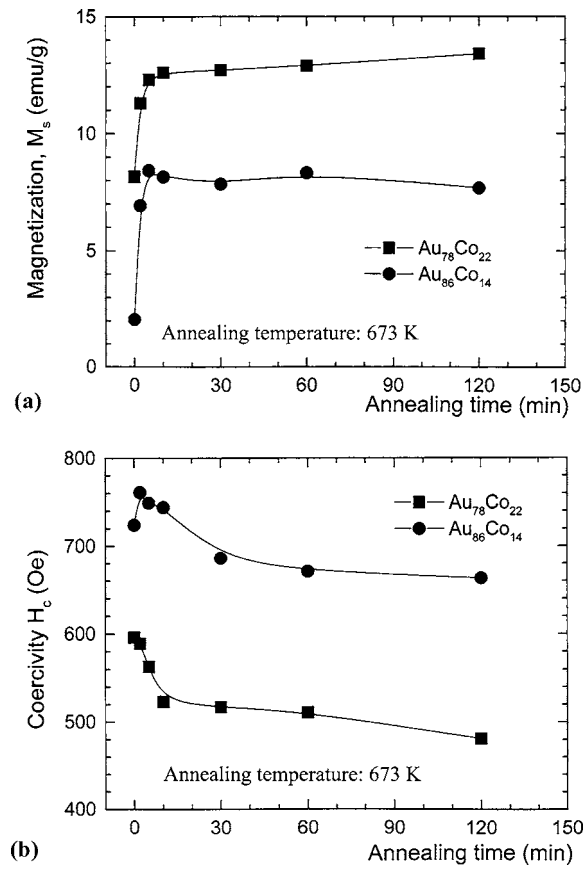

Figure 11 The magnetic properties of $Au_{78}Co_{22}$ and $Au_{86}Co_{14}$ (measured at room temperature) as a function of annealing time at 673 K: (a) Saturation magnetization (M_s) and (b) Coercivity (H_c).

particles and medium magnetic fields were used, superparamagnetic to ferromagnetic transition of some Co precipitates could also contribute to the saturation increase. The saturation magnetization of both samples was approximately constant, with only a slight decrease at temperatures above 723 K.

After annealing at 873 K for 10 min, the saturation magnetization (M_s) of $Au_{86}Co_{14}$ was 7.3 emu/g and that of $Au_{78}Co_{22}$ was 12.9. Ignoring the small amount of Co dissolved in the Au matrix after annealing at 873 K for 10 min and assuming that all Co precipitates are ferromagnetic, it can be seen that the value of the saturation magnetization is directly related to the amount of the ferromagnetic Co precipitates [9]. The ratio $M_s(Au_{86}Co_{14})/M_s(Au_{78}Co_{22}) = 7.3/12.9 = 0.57 \approx 0.61 = 4.69/7.69 = \text{wt\%Co}(Au_{86}Co_{14})/\text{wt\%Co}(Au_{78}Co_{22})$ (measured by wet chemical analysis).

The coercivities of both samples decreased gradually with the increase in annealing temperature, which correlate with the measured growth of Co precipitates (Fig. 10b). The coercivity of the $Au_{86}Co_{14}$ alloy first increased after 2 min annealing at 673 K and then decreased with the increase in the annealing time (Fig. 11b). The Co precipitates in the as-cast $Au_{86}Co_{14}$ alloy were smaller (20–35 nm) than the estimated critical size for a single magnetic domain of fcc Co (30–60 nm [6]). Thus it is expected that due to the coarsening of the Co precipitates, the coercivity first increases as the Co precipitates approach the critical single domain size and then decreases when the Co precipitates exceed the single-domain size. The coercivity of the $Au_{78}Co_{22}$ alloy decreased with increased annealing time, since most of the Co precipitates in the as-cast alloy were 50–70 nm, which are close to or even larger than the critical single domain size.

3.3. GMR

3.3.1. $Au_{78}Co_{22}$

The magnetoresistance (MR) ratio was defined as $\Delta\rho/\rho_{14.5\ \text{kOe}} = (\rho_H - \rho_{14.5\ \text{kOe}})/\rho_{14.5\ \text{kOe}}$, where ρ_H and $\rho_{14.5\ \text{kOe}}$ are the resistances of the sample in an applied magnetic field of H and 14.5 kOe, respectively. MR ratio ($\Delta\rho/\rho$) as a function of the magnetic field (H), of the as-cast and the annealed (at 673 K for 1 hr) $Au_{78}Co_{22}$ alloy, are shown in Fig. 12a. As can be seen from Fig. 12a, the $\Delta\rho/\rho$ curve of the as-cast $Au_{78}Co_{22}$ alloy has two distinct regions: a part with a relatively rapid decrease of the $\Delta\rho/\rho$ in small magnetic fields (-2 kOe $< H <$ 2 kOe) and a part with a smaller and changing slope in higher magnetic fields. Similar behavior was reported for a melt-spun $Au_{71.6}Co_{28.4}$ [9]. Since wide range of precipitate's sizes exist in the as-cast alloy it is hard to know the contribution of each size group to GMR. Also, there are other factors that influence GMR such as the spacing between the precipitates and also, according to Vrenken *et al.* [12], the coherency between the Co precipitates and the Au matrix. However, based on reported experimental works [9, 12, 18], we can give a possible explanation. Vrenken *et al.* [12] found that the main contributor to GMR of water quench of solid-solution $Au_{80}Co_{20}$ was small coherent Co precipitates dispersed homogeneously in the grains. While Hütten

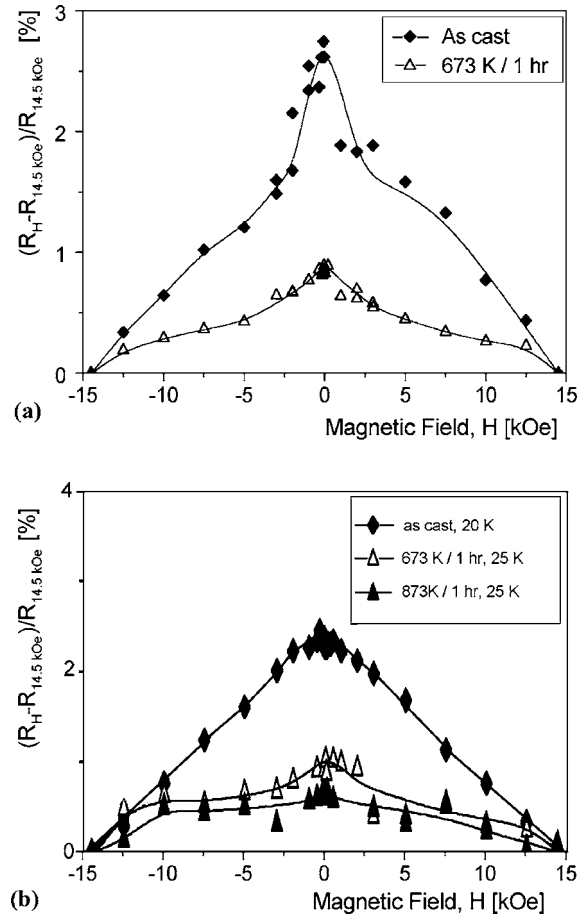

Figure 12 Magnetoresistance ratio ($\Delta\rho/\rho$) versus magnetic field, H, of as-cast and annealed $Au_{78}Co_{22}$ (a) and $Au_{86}Co_{14}$ (b) alloys.

et al. [9] attributes the GMR effect observed in melt-spun $Au_{71.6}Co_{28.4}$ to the lamellar structure. As will be given later, the $Au_{86}Co_{14}$ didn't show GMR and had almost no lamellar structure. So the central part of the Fig. 12a, showing GMR, may be connected to the lamellar structure. Musa reported that large magnetic fields, usually on the order of tens of kOe, are needed to align the magnetic moments of the superparamagnetic Co precipitates in a Cu–Co system [19]. Our experiment was conducted in magnetic fields up to 14.5 kOe, which is probably not enough to saturate the Co precipitates. Therefore, the small superparamagnetic Co precipitates (with wide size distribution; Fig. 3) could be connected to the long unsaturated tail in higher magnetic fields (MR behavior) in Fig. 12a.

Annealing at 673 K for 1 hr caused $\Delta\rho/\rho$ to fall from 2.6% to about 0.9 % (see Table II). The shape of the $\Delta\rho/\rho$ curve of the annealed sample resembles that of the as-cast sample, but the steepness of the central part of the curve is much less dominant.

TABLE II MR ratio ($\Delta\rho/\rho$) of Au–Co alloys. All the measurements were performed at temperature of 20–25 K

	MR ratio (%)		
Alloy	As-cast	673 K/1 hr annealed	873 K/1 hr annealed
$Au_{78}Co_{22}$	2.6	0.9	–
$Au_{86}Co_{14}$	2.5	1.0	0.7

There are a few reasons for the $\Delta\rho/\rho$ reduction. As the Co precipitates and lamellae grew, as shown in Fig. 7, the surface/volume ratio decreased, reducing the spin-dependent interfacial scattering (the main contributor [9] to GMR), relative to the bulk scattering effect [8]. In addition, due to the annealing [9], the precipitates became larger than the mean free path within the precipitates. Vrenken [12] reported that loss of coherency between the small Co precipitates and the Au matrix upon annealing is the main reason for the decrease in GMR. On the other hand, Krishnan [20] explained the decrease of GMR, after annealing of multilayered permalloy, as due to roughening of the interface between the ferromagnetic and the non magnetic layers.

Finally, when the precipitates exceeded the critical size d_c and were no longer single domains, the interaction of the conduction electron spins with the varying magnetization distribution in the Co precipitates produced a state in which the conduction electron spin channels were mixed [8]. The estimated critical diameter d_c for single magnetic domain in fcc Co was 30–60 nm (the uncertainty in the diameter results from the lack of accurately in the known magnetic parameters of fcc Co at room temperature) [6]. As was reported earlier, the size of most of the Co precipitates in as-cast $Au_{78}Co_{22}$ alloy was 50–70 nm, which is perhaps above the d_c. However, Lorentz TEM of the as-cast $Au_{78}Co_{22}$ alloy found that all the examined Co precipitates were single magnetic domain.

On the other hand, as shown above, annealing also causes the removal of Co from the Au matrix, which reduces the scattering impurities (Co) and increases the mean-free path. This should lead to an increase in the GMR [21] and indeed Helmot *et al.* [10] reported that annealing at 603 K for 1 hr improved $\Delta\rho/\rho$ of melt-spun $Au_{80}Co_{20}$ from 0.6% (as-cast) to 2%. It is thus concluded that our sample was already decomposed or needed a gentler annealing treatment (lower temperatures and/or shorter annealing times) in order to achieve maximum GMR.

3.3.2. $Au_{86}Co_{14}$

Fig. 12b shows the $\Delta\rho/\rho$ as a function of the magnetic field, of the as-cast and the annealed (1 hr at 673 K and 873 K) $Au_{86}Co_{14}$ alloy. The shape of the as-cast $Au_{86}Co_{14}$ alloy curve differs substantially from that of the as-cast $Au_{78}Co_{22}$ alloy discussed above. Here, $\Delta\rho/\rho$ changes almost linearly with the applied magnetic field (H) with no saturation, suggesting that most of the Co precipitates are superparamagnetic [4, 9]. Indeed, very small Co precipitates (below $D_c = 3.8$ nm at room temperature [6]), seen only by strain contrast, were present in the $Au_{86}Co_{14}$ alloy. The $\Delta\rho/\rho$ value of the as-cast $Au_{86}Co_{14}$ alloy was 2.5%, which is similar to that of the as-cast $Au_{78}Co_{22}$, although there were differences in both composition and microstructure.

Below a certain blocking temperature (T_B), the superparamagnetic precipitates are 'blocked', which mean they are no longer superparamagnetic. T_B depends on the size of the precipitates. Thus, at any given temperature only a fraction of the magnetic Co precipitates will be superparamagnetic (unblocked), while the remainder will not be superparamagnetic (blocked). Since the MR measurements were performed at 25 K there is a good possibility of blocked Co precipitates.

One hour annealing of the as-cast $Au_{86}Co_{14}$ alloy at 673 K and 873 K caused the decrease in $\Delta\rho/\rho$ from 2.5% to 1% and 0.7%, respectively. The curves of $\Delta\rho/\rho$ as a function of H of the annealed $Au_{86}Co_{14}$ were not linear as in the as-cast alloy, but had a similar shape to the annealed $Au_{78}Co_{22}$ alloy. This means that the superparamagnetic nature of the alloy had been changed and some of the precipitates had grown and had become ferromagnetic, which was indeed observed in TEM.

4. Summary

The microstructure and the chemical composition of melt-spun Au–Co alloys were investigated by TEM, HRTEM and analytical TEM. The microstructure of $Au_{86}Co_{14}$ was composed of very small Co precipitates dispersed inside Au grains with some larger Co precipitates (20–35 nm) dispersed at the grain boundaries. The microstructure of the $Au_{78}Co_{22}$ alloy consisted of Au/Co lamellar eutectic grains with Co precipitates (50–70 nm) dispersed at the grain boundaries. A few grains had very small Co precipitates (4 nm). Microanalysis showed that the Au matrix contained 5.4–10.0 at.% Co, which decreased to 0.9–2.0 at.% after annealing at 773 K for 10 min. The reduction of the Co concentration in the Au matrix was accompanied by Co precipitation and enlargement of other Co precipitates and lamellae.

Lorentz TEM imaging showed that both the Co precipitates and lamellae had a single-domain magnetic structure. Annealing caused the transition of single-to multi-domain magnetic structure.

The coercivity of $Au_{86}Co_{14}$ increased after the first 2 min of annealing at 673 K and then decreased with the increase in annealing time, while the coercivity of $Au_{78}Co_{22}$ decreased with the annealing time. The initial increase in coercivity of the $Au_{86}Co_{14}$ alloy was due to the formation of single-domain Co precipitates at the grain boundaries. Coarsening of the Co precipitates and transition to a multi-domain magnetic structure caused the decrease of coercivity for both alloys. The saturation magnetization of both samples annealed at 673 K also increased with the increase in annealing time and reached plateau after 10 min. These changes are consistent with removal of Co from the Au matrix.

The change of $\Delta\rho/\rho$ with the applied magnetic field of the as cast $Au_{86}Co_{14}$ alloy was linear with no saturation, suggesting superparamagnetic behavior of the very small Co precipitates. The shape of the $\Delta\rho/\rho$ curve of the as-cast $Au_{78}Co_{22}$ alloy had two distinct regions. A part with a relatively rapid decrease of the $\Delta\rho/\rho$ in small magnetic fields (-2 kOe $< H <$ 2 kOe), possibly connected to the lammelar structure, and a part with a smaller slope in higher magnetic fields, attributed to the small ferromagnetic/superparamagnetic Co precipitates. The $\Delta\rho/\rho$ values (in 14.5 kOe field) of the as-cast $Au_{86}Co_{14}$ and $Au_{78}Co_{22}$ alloys were 2.5% and 2.6%, respectively.

Annealing at 673 K temperature for 1 hr caused a reduction in the magnetoresistance to 1% or less. This reduction in GMR can arise from several causes associated with Co particle coarsening. These include: the decrease in surface to volume ratio which reduces spin dependent interfacial scattering; an increase in size which exceeds the mean free path; interfacial roughening; and probably most important, the transition from single to multi-domain structures.

Acknowledgements

This work was supported by the Director, Office of Basic Energy Sciences, Division of Materials Sciences of the United States Department of Energy under Contract No. DE-AC-03-76SF00098. The authors would like to thank C. Echer, R. Kilaas, C. Nelson, C.Y. Song and E. Stach from NCEM, and Dr. E. Girt, now at Seagate Technology, for experimental help and fruitful discussions. Dr. V. Markovich, from the Department of Physics in Ben-Gurion University, is acknowledged for assistance with magnetoresistance measurements.

References

1. M. N. BAIBICH, J. M. BROTO, A. FERT, F. NGUYEN VAN DAU, F. PETROFF, P. EITENNE, C. CREUZET, A. FRIEDERICH and J. CHAZELAS, *Phys. Rev. Lett.* **61**(21) (1988) 2472.
2. P. M. LEVY, *Sol. Stat. Phys.* **47** (1994) 367.
3. J. Q. XIAO, J. S. JIANG and C. L. CHIEN, *Phys. Rev. Lett.* **68**(25) (1992) 3749.
4. A. E. BERKOWITZ, J. R. MITCHELL, M. J. CAREY, A. P. YOUNG, D. RAO, A. STARR, S. ZHANG, F. E. SPADA, F. T. PARKER, A. HÜTTEN and G. THOMAS, *J. Appl. Phys.* **73** (1993) 5320.
5. C. L. CHIEN, J. Q. XIAO and J. S. JIANG, *J. Appl. Phys.* **73**(10) (1993) 5309.
6. J. BERNARDI, A. HÜTTEN and G. THOMAS, *Nanostructured Materials* **7** (1996) 205.
7. J. BERNARDI, A. HÜTTEN, S. FRIEDRICHS, C. E. ECHER and G. THOMAS, *Phys. Stat. Sol.* (a) **147** (1995) 165.
8. A. E. BERKOWITZ, J. R. MITCHELL, M. J. CAREY, A. P. YOUNG, S. ZHANG, F. E. SPADA, F. T. PARKER, A. HÜTTEN and G. THOMAS, *Phys. Rev. Lett.* **68**(25) (1992) 3745.
9. A. HÜTTEN, J. BERNARDI, S. FRIEDRICHS and G. THOMAS, *Scripta Met.* **33** (1995) 1647.
10. R. V. HELMOT, J. WECKER and K. SAMWER, *Appl. Phys. Lett.* **64**(6) (1994) 791.
11. C. G. LEE, S. H. KIM, D. H. LEE and K. FUKAMICHI, *IEEE Trans. Magn.* **35**(5) (1999) 2856.
12. H. VRENKEN, B. J. KOOI and J. TH. M. DE HOSSON, *J. Appl. Phys.* **89**(6) (2001) 3381.
13. N. KATAOKA, H. TAKEDA, J. ECHIGOYA, K. FUKAMICHI, E. AOYAGI, Y. SHIMADA, H. OKUDA, K. OSAMURA, M. FURUSAKA and T. GOTO, *J. Magn. Magn. Mater.* **140–144** (1995) 621.
14. H. OKAMOTO, T. B. MASSALSKI, M. HASEBE and T. NISHIZAWA, *Bull. Alloy Phase Diagrams* **6**(5) (1985) 449.
15. R. A. YOUNG, A. SAKTHIVEL, T. S. MOSS and C. O. PAIVA-SANTOS, *J. Appl. Cryst.* **28** (1995) 366.
16. J. BERNARDI, A. HÜTTEN and G. THOMAS, *J. Magn. Magn. Mater.* **157/158** (1996) 153.
17. M. F. ASHBY and L. M. BROWN, *Phil. Mag.* **8** (1963) 1083 & 1649.
18. O. REDON, J. PIERRE, B. RODMACQ, B. MEVEL and B. DIENY, *J. Magn. Magn. Mater.* **149** (1995) 398.
19. S. O. MUSA, M. A. HOWSON, B. J. HICKEY and N. WISER, *J. Magn. Magn. Mater.* **148** (1994) 309.
20. K. M. KRISHNAN, *Acta Mater.* **47**(15) (1999) 4233.
21. S. ZHANG and P. M. LEVY, *J. Appl. Phys.* **73**(10) (1993) 5315.

Received 21 June 2002
and accepted 26 February 2003